

Evidence for Quantisation in Planetary Ring Systems

R. Wayte

29 Audley Way, Ascot, Berkshire SL5 8EE, England, UK.

e-mail: rwayte@googlemail.com

Research article, Submitted to PMC Physics A. 25 Nov 2009

Abstract

Absolute radial positions of the main features in Saturn's ring system have been calculated by adapting the quantum theory of atomic spectra. Fine rings superimposed upon broad rings are found to be covered by a harmonic series of the form $N \propto A(r)^{1/2}$, where N and A are integers. Fourier analysis of the ring system shows that the spectral amplitude fits a response profile which is characteristic of a resonant system. Rings of Jupiter, Uranus and Neptune also obey the same rules. Involvement of the atomic fine structure constant throughout implies the existence of a real quantisation force linking gravitation and atomic theories.

PACS Codes: 96.12.Uv, 96.30.Mh, 96.30.Wr.

1. Introduction

It is not true that the ring system of Saturn has now been fully explained in classical terms, see comments by Cuzzi et al [1], pp215-6, Esposito [2], pp1743, 1750-1, 1777, Gordon et al [3], pp265, 281.

Given the appearance of Saturn's rings (Figure 1), some broad and diffuse others very narrow but dense, it seemed reasonable to apply some of the established rules governing atomic spectra. Inevitably, quantum theory must apply to everything, so direct application to this macro-system is sensible. These atomic rules have been adapted here to fit PPS optical depth ring data, by introducing the gravitational constant G and astronomical masses in place of equivalent electromagnetic factors. A hierarchical system has thereby been revealed, which represents a multiple link between gravitation and atomic theories.

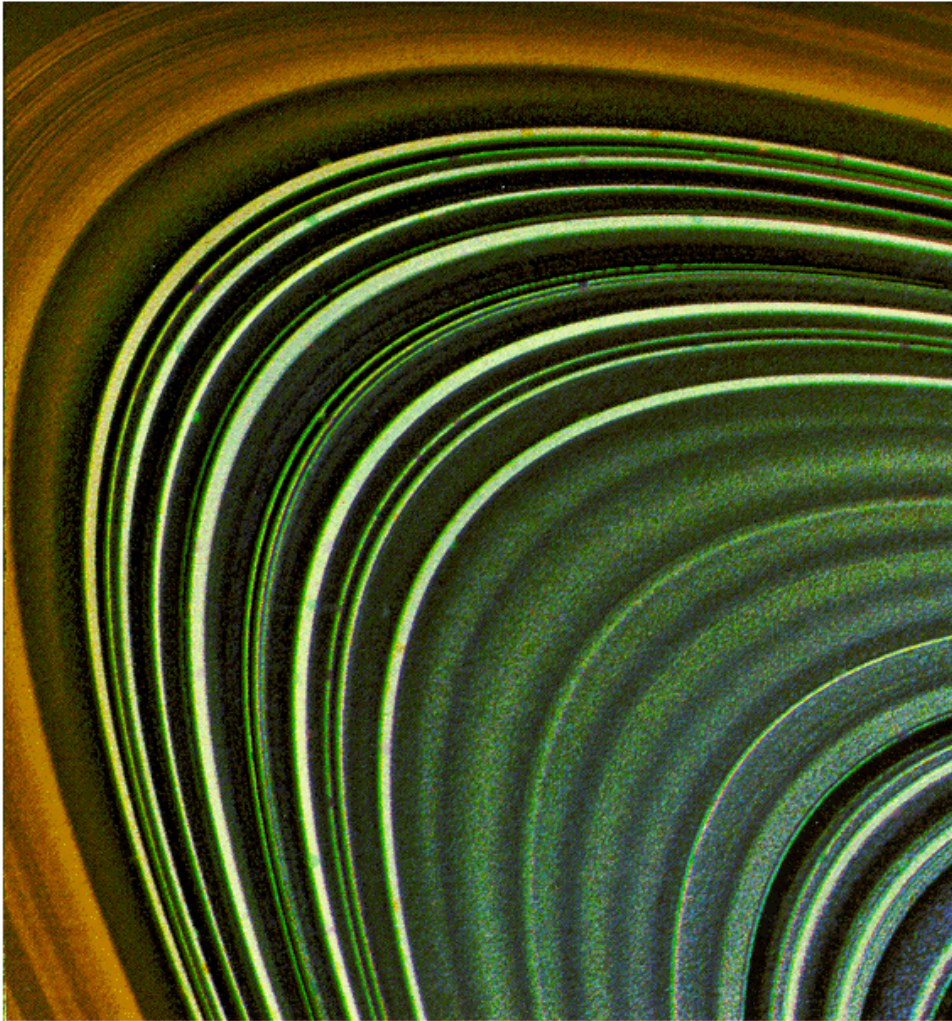


Figure 1. Composition image of Saturn's C Ring showing weak broad diffuse rings superimposed by strong narrow rings. Courtesy, NASA at http://ringmaster.arc.nasa.gov/saturn/voyager/plate_06.gif

Many aspects of the Saturnian ring structure recorded by Pioneer and Voyager spacecraft have been published, such as the multitude of broad and narrow rings obeying no simple laws, regions of density waves and resonance peaks or gaps caused by moons. See Cuzzi et al. [4]; Lissauer et al. [5]; Goldreich and Tremaine [6]; Holberg et al. [7]; Smith et al. [7]; Esposito et al. [8]; Lane et al. [8]; Cuzzi et al. [9]; Borderies et al. [10]; Esposito [11]; Borderies [12]; Esposito et al. [13]; Nicholson and Dones [14]; Nicholson [15]; Horn and Cuzzi [16]; Fridman [17]; Nicholson [18]; Esposito [19]; Gordon et al. [20]; Tiscareno et al. [21]. Some rings have been identified with density waves and resonances due to moons, satellites and Saturn's oblateness. However, the vast complexity of very fine rings superimposed upon broad

rings has not been covered by an overall theory. The origin or reason for the rings remains an outstanding problem. In addition, the observed rings around Uranus, Neptune and Jupiter need to be included in a single viable theory.

This work may be compared with other interesting papers already published on the apparent quantisation of orbits in the Solar System; see for example, Wayte [22], Nottale et al. [23], Rafie [24]. It is not related to Bode's law, which has no physical foundation or accuracy to recommend it. Neither is it numerology, any more than the original Balmer Series published in 1885 was.

2. Quantisation

All atomic spectra are governed by the electromagnetic coupling constant (atomic fine structure constant):

$$\alpha = \frac{e^2}{\hbar c} \approx \frac{1}{137} , \quad (1)$$

where e is the electronic charge, \hbar is Planck's constant divided by 2π , and c is the velocity of light. If there is ever to be a quantum theory of gravity which is compatible with electromagnetic quantum theory, then we should expect this coupling constant to appear in all manner of astronomical contexts. Remarkably, for Saturn there is an analogous coupling constant for gravity involving the hydrogen molecular mass m_{H_2} and Saturn's mass $M_S = 568.46 \times 10^{24} \text{ kg}$:

$$\frac{GM_S m_{H_2}}{\hbar c} \approx \alpha \times \left(\frac{e^2}{G m_{H_2}^2} \right)^{1/2} . \quad (2)$$

The final term represents a ratio between gravitational and electromagnetic forces for H_2 . This expression could be a record of some cosmogonic quantum process which helped determine the mass of Saturn during its condensation from the original solar nebula. We shall see that this particular expression for Saturn contributes very well towards explaining the ring dynamics, and could even account for the uniqueness of Saturn's ring system.

The aim in this section is therefore to identify rules that are known to operate within atomic systems, which can be applied to Saturn's rings. For example, every Bohr orbit of hydrogen has an integral number of de Broglie wavelengths around it:

$$2\pi r = N \left(\frac{h}{mv} \right) , \quad (3a)$$

where m is the electron mass, v is its velocity, and N is the principle quantum number. So these orbits are quantised and may be numbered from the center as:

$$N = \left(\frac{1}{137} \right) \left(\frac{c}{v} \right) = 1, 2, 3, \dots, \infty \quad , \quad (3b)$$

where c is the velocity of light. This formula has been applied directly to Saturn's rings with N defined analogously as ring number, and v the ring material orbital velocity. Clearly N cannot be seen from unity because Saturn is in the way, but it is observed immediately at the inside of the D Ring and carries on to the F Ring. Given Eq.(2) and Eq.(3b), the analogy to Eq.(3a) for Saturn is:

$$2\pi r = N \left(\frac{h}{m_{H_2} v} \right) \times \left(\frac{e^2}{G m_{H_2}^2} \right)^{1/2} \quad . \quad (3c)$$

There is no known *classical* reason for such direct analogy between atomic orbits and Saturn's rings.

In addition to this fundamental quantisation rule, there are various harmonics described by:

$$N = \frac{A}{137} \left(\frac{c}{v} \right) \quad , \quad (4)$$

where A is always an integer. These fit a multitude of fine rings between the principle rings, with more than enough correlation to infer that a *quantisation effect* is operating around orbits to produce and *maintain* the separate rings. In atomic theory, Eq.(3a) is connected with a probability *amplitude*, but Eq.(3c) for the rings covers *intensity* of the quantisation and might explain orbital clumping of material, in the form of a standing-wave. Such a standing-wave would be inherently stable over a long period. There is no reason why more rules, for particle masses other than m_{H_2} , should not compete simultaneously for ring material and produce complex ring systems.

For the data analysis, we will assume circular Keplerian orbits ($GM_S = v^2 r$), and find it better to express Eq.(4) in terms of the measured ring radius:

$$N = \frac{A}{137} \left(\frac{c^2}{GM_S} \right)^{1/2} r^{1/2} \quad . \quad (5)$$

Consequently, the PPS optical depth data, supplied by NASA at http://ringmaster.arc.nasa.gov/cds/VG_2801/EASYDATA/KM005/ has been reduced to (radius)^{1/2} format. This data [in 14,101 bins of 5 km spacing, from ring radius $r = 72,000$ km to 142,500 km], has been transformed using the formula:

$$x = (r \times 11,520.4)^{1/2} - 28,799.5 \quad . \quad (6)$$

These calculated 14,101 non-integral values of x were rounded to the nearest integer, whereupon duplicate values were removed, leaving 11,718 bins of data in *integral* x values, as plotted in Figure 2. Integral values of \mathbf{N} will then be spaced linearly along the abscissa, aligned with their corresponding rings.

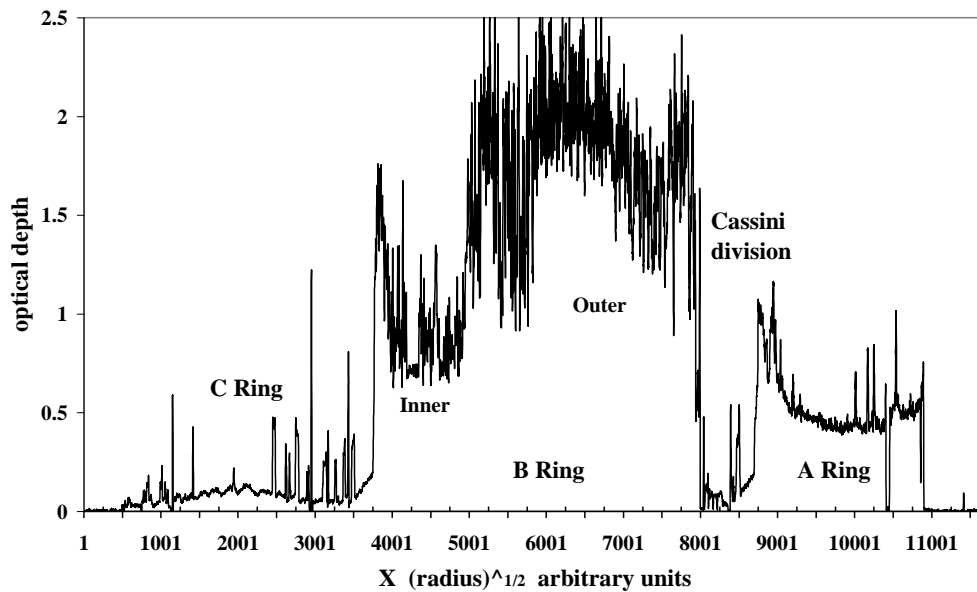


Figure 2. Saturn's ring system, plotted as optical depth versus variable x given by Eq.(6). Original PPS 5 km resolution data have been smoothed over 7 bins for clarity.

One aspect of great importance is that \mathbf{N} is *absolute*, starting from zero at the centre of Saturn. This means that Eq.(5) has to fit all the rings in the system simultaneously without the benefit of local adjustments. Sharp edges and horns of many strong rings are also found to fit, as if the quantisation phenomenon influences ring structures as well as positions. Another important aspect is that every theoretical ring position need not be occupied because the available material could have been coerced into adjacent orbits by moons or turbulence.

When fitting some of the fine rings it is also observed that Eq.(4) may be expressed in terms of a *gravitational Compton* wavelength Λ_{GC} in addition to a de Broglie wavelength Λ_{GB} . That is, for molecular hydrogen participation, we have:

$$N \times 137 \left(\frac{h}{m_{H_2} c} \right) \left(\frac{e^2}{G m_{H_2}^2} \right)^{1/2} = A \left(\frac{h}{m_{H_2} v} \right) \left(\frac{e^2}{G m_{H_2}^2} \right)^{1/2} ,$$

or:

$$N \times 137 \Lambda_{GCH_2} = A \Lambda_{GBH_2} . \quad (7)$$

This means that material will accumulate in rings where Compton and de Broglie wavelengths are *commensurable* around an orbit. When an orbit circumference is equal to an integral number of Compton gravitational wavelengths, single valued quantisation occurs and may even encourage localised clumping of material around the orbit. From Eqs.(2) and (7) we can derive an informative numerical relationship:

$$2\pi r \approx 137 \left(\frac{N}{A} \right)^2 \Lambda_{GCH_2} . \quad (8)$$

So, theoretically, between the F Ring ($N \approx 133$, $A = 1$) and the inner D Ring ($N \approx 92$, $A = 1$) there are 1,264,000 allowed ring positions at typical separation 0.06 km. This covers the 'record-groove' structure pervading Saturn's dense rings.

Generally, broader or stronger ring features employ lower values of coefficient **A**. In addition, any *very sharp increase* in opacity at a ring border is often associated with a horn profile which also fits the quantisation rule. Consequently, the quantisation force must be physically real rather than being an artifact of some other influence. However, the force is still relatively weak and easily overcome by bulk turbulence, so rings do not form at all in some regions. Material may also be moved by normal satellite perturbations, leading to the ring pattern changing regularly in detail. There is evidence to indicate that the moons act like clumps and satisfy the quantisation rules, as will be demonstrated for the Encke and Keeler gaps.

Before proceeding with the extensive application of Eq.(5) to the rings, it is interesting to apply de Broglie's equation directly to the whole system, in a way analogous to the hydrogen atom. For the Bohr orbits of hydrogen we have:

$$2\pi r = n \left(\frac{h}{mv} \right) = n \lambda_B , \quad (9)$$

where **n** is an integer and ($\lambda_B = h/mv$) is the electronic de Broglie wavelength. For Saturn's rings there is a direct gravitational analogy:

$$2\pi r = S \left[\left(\frac{h}{m_p v} \right) \times \left(\frac{e^2}{G m_p^2} \right)^{1/2} \right] = S \Lambda_{GBP} , \quad (10)$$

where Λ_{GBp} is the effective *gravitational de Broglie* wavelength of protons (mass m_p) in ring material. Here S is expected to be integral where the ring material accumulates most strongly, as confirmed in Figure 3; although the *self-gravitation force* of the material has caused filling between rings. The resonance phenomenon causing the Cassini division has overridden the accumulation force.

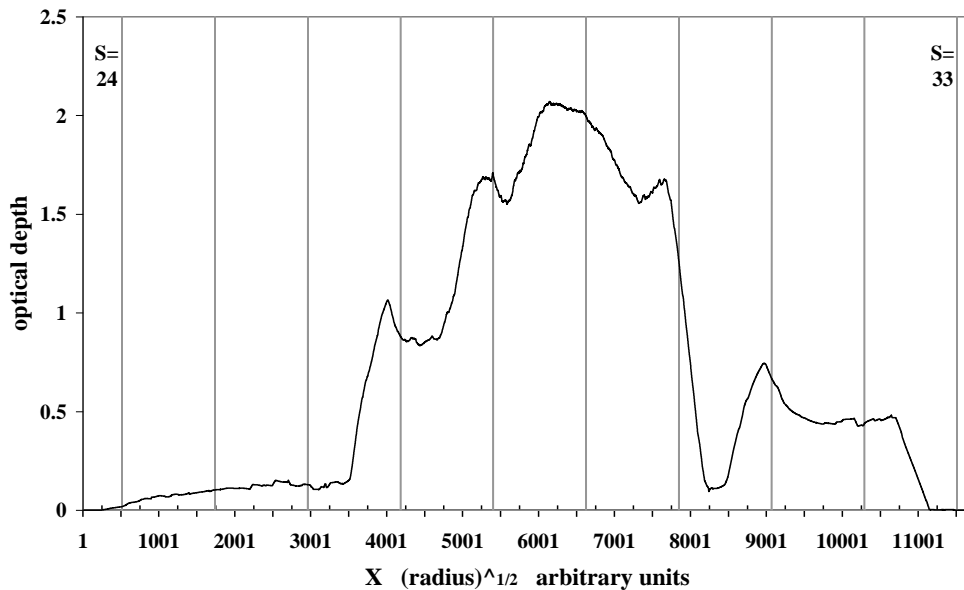


Figure 3. Fundamental periodicity in the ring system, revealed by smoothing over 500 bins. The vertical markers represent integral values of S from 24 to 33, derived from Eq.(10).

3. Analysis of Saturn's C Ring

In order to view the low-level broad diffuse rings, all strong narrow rings were compressed in optical depth as shown in Figure 4. A moving box-car smooth over 15 bins was then performed to clarify the low-frequency fit of quantisation rule Eq.(5). Periodicity is illustrated in the good fit of rings for $A = 1, 2, 4, 8$, as marked at the bottom. The fit for $A = 3, 6, 9, 12$, is marked at the top, where some of the $A = 3$ markers must correspond with values for $A = 1$. Only eight values of A are necessary to describe 32 major rings, not counting this overlap. The way that the rings in the central region change from $A = 1, 2$, to $A = 1, 3$ implies that these two quantisation schemes are competing for material and "beating" in the well-known manner. In each set, the lowest possible A value is marked. This excellent fit of Eq.(5) to data is

critical, given that A is absolute and therefore highly sensitive to observed r and M_S values.

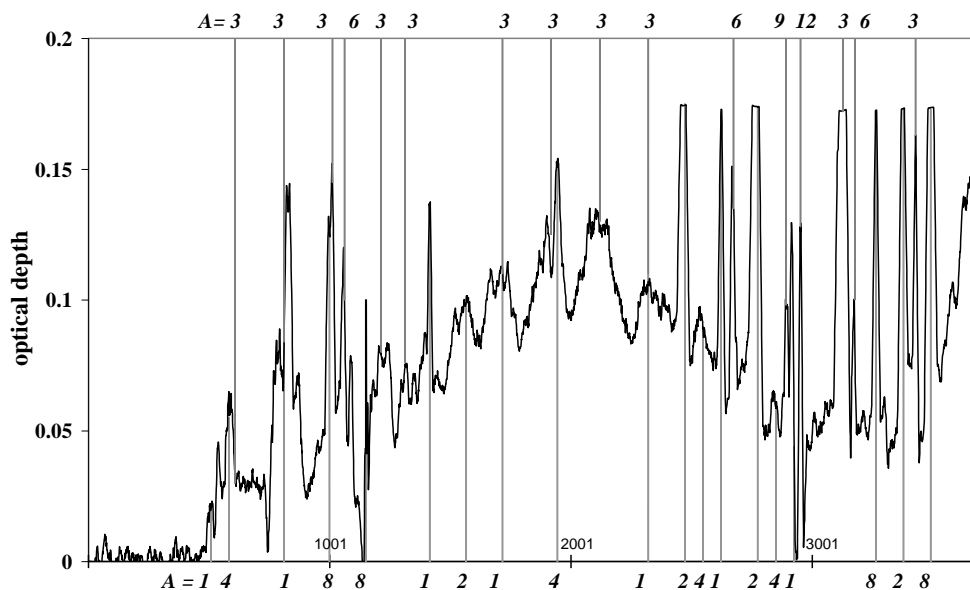


Figure 4. Optical depth profile of the C Ring from $x = 1$ to 3700, after attenuating the very strong narrow rings. Lower markers are situated for coefficient $A = 1, 2, 4, 8$, in alignment with diffuse and narrow rings. Upper markers are for $A = 3, 6, 9, 12$. Data have been smoothed over 15 bins for clarity.

Fourier transformation of the *complete C Ring* data was found to be dominated by the strong narrow rings, so these were truncated. The subsequent transform was still not very useful because periodicity in A is broken by the many vacant N values. Consequently, in order to reveal *local A* values, the C Ring was Fourier transformed in 12 sections of 256 bins each. Pairs of these transforms were then summed to reduce errors, giving 6 spectra for 6 adjacent regions in the C Ring, see Figure 5. Although these differ from region to region, the *overall mean* spectrum is relatively smooth and has the characteristic form of a mechanical resonant system (see Stephenson, [25]). The low frequency cut-off is due to the Fourier sampling of only 256 bins, but the decay at higher frequencies is inherent in the data. A calculated resonance response profile is shown dotted, and given by:

$$y = y_o Q \left[1 + Q^2 \left(\frac{A}{A_o} - \frac{A_o}{A} \right)^2 \right]^{-1/2}, \quad (11)$$

where $y_0 = 1.25$, $A_0 = 1$, and $Q = 0.75$ is a measure of stored energy relative to energy losses. In this context, the losses are significant and may be interpreted as viscous due to turbulence, which impedes the quantisation process. Evidently, this good overall fit shows that the ring quantisation phenomenon is not random, and has features analogous to electro-mechanical systems.

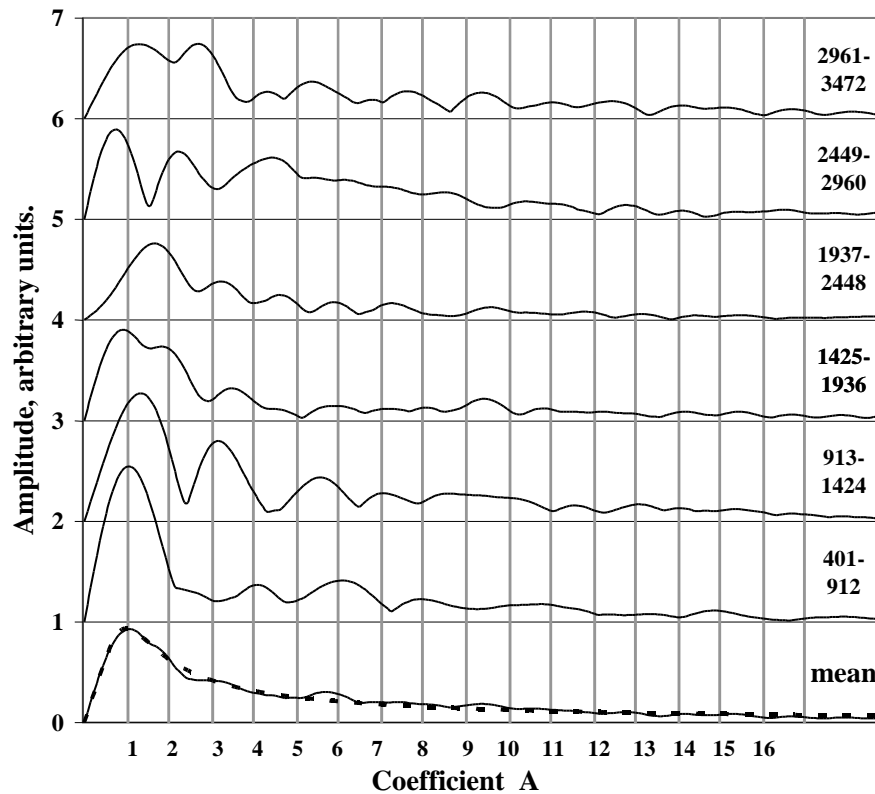


Figure 5. Fourier spectra of 6 adjacent regions in the C Ring. Considerable variation is apparent between spectra but the *mean* spectrum approximates to a resonance response profile.

The complex inner C Ring data, from bin 481 to 1141, was subjected in more detail to the quantisation rule Eq.(5). Figure 6 illustrates the fit of 40 ring positions for only 10 chosen values of A , from 3 to 48. Coefficient A can change easily, because the quantisation force decreases only slowly as A increases, according to Eq.(11). Rings would have then formed from chaotic material via the most energy efficient route, allowing for perturbations due to moons and other rings. Certain values of A clearly reveal harmonic periodicity. For example, the three narrow rings at $(x = 293, A = 8)$ $(x = 306, A = 12)$ $(x = 318, A = 24)$ are equally spaced and could all be grouped into $(A = 24)$. The neighbouring strong ring at $x = 350$ covers 5 equally

spaced rings satisfying ($A=12, 16, 24, 48$) or equally ($A = 48$) for all, which have been filled by self-gravity. The low noise level for the data is shown at the left end.

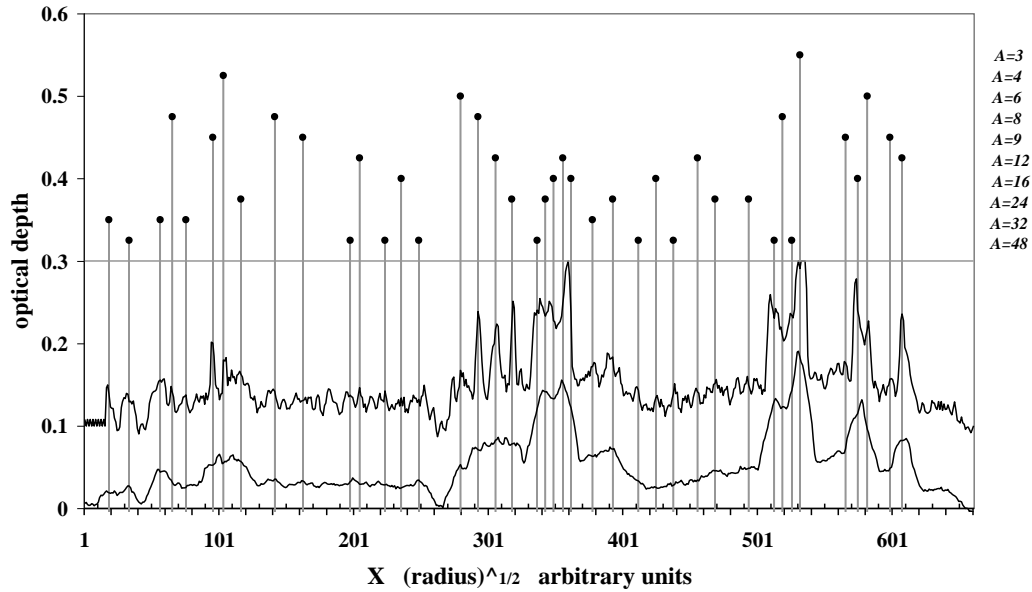


Figure 6. Upper trace: Inner C Ring data smoothed over 3 bins and analyzed to discover the values of A listed on the right. The noise level is indicated at the left end of the data. Lower trace: Smoothing over 13 bins is also included to show how the finer rings are undetected at lower spatial resolution.

There is one particularly narrow strong ring at radius 90,193 km ($x = 3435$ in Eq.(6)) associated with the Mimas 3:1 resonance, which has been studied by Lane et al.[10] because of its pronounced superimposed fine ringlets of radial width 2 km. For these ringlets, there is an observed transition from Eq.(4) to a finer form:

$$N = B(c/v) \quad . \quad (12a)$$

Here, B is an integer, so this confirms another tight *absolute* connection between the Compton and de Broglie gravitational wavelengths around each ring, analogous to Eq.(7), namely:

$$N\Lambda_{GC} = B\Lambda_{GB} \quad . \quad (12b)$$

Equation (12a) has been applied to this feature and describes the *absolute positions* of the ringlets remarkably well, as shown in Figure 7. The ring data has 1 km resolution and was supplied by NASA at

http://ringmaster.arc.nasa.gov/cds/VG_2801/EASYDATA/KM001/PS1P0109.TAB.

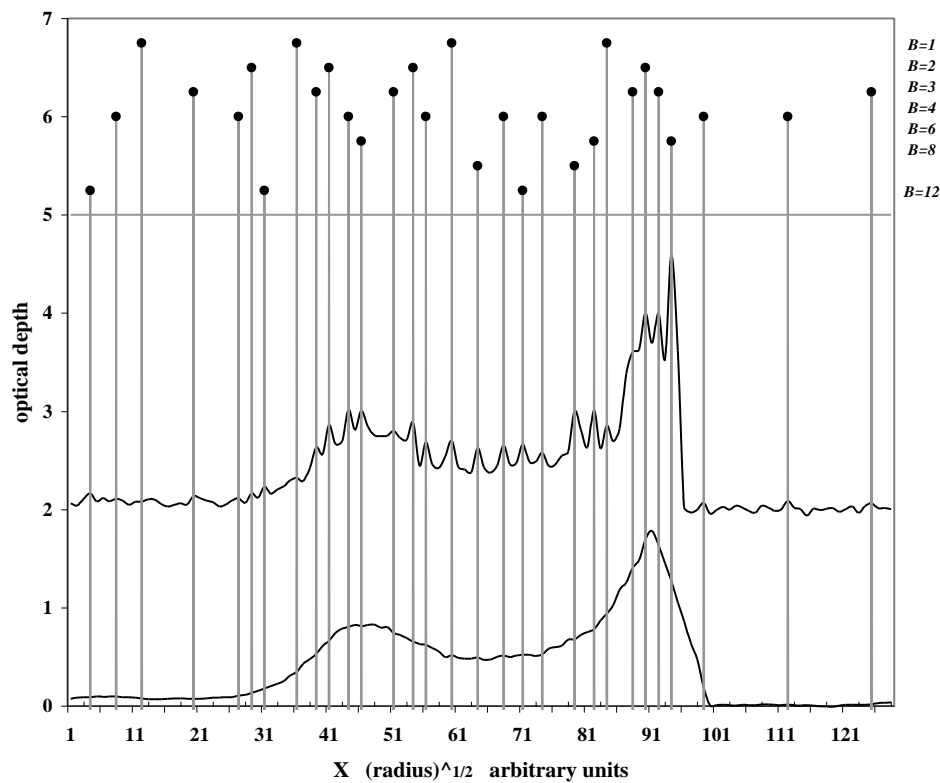


Figure 7. Upper trace: The feature at radius 90193 km analyzed at high resolution (1 km). Increased resolution would probably separate these fine rings further. The B values from Eq.(12a) are given at top right. Lower trace: The same feature at lower resolution (5km).

Even higher resolution would be advantageous in future work because these ringlets appear not fully resolved. In order to make the ringlet spacing linear as previously, this higher resolution raw data batch was transformed using the formula:

$$x = (r \times 360,000)^{1/2} - 179,999 \quad . \quad (13)$$

Figure 7 covers the short range from bin 101 to 228, with high values of B describing the finest rings upon broader rings. Again, fitted values of B are found to be multiples of 2 and 3, implying resonance couplings between ringlets.

In the outer part of the C Ring ($x = 2400-3600$ in Figure 4) there are some very strong narrow rings with exceptionally rapid increase in opacity at their edges, see Figure 8. Horns indicate a controlling implementation of the quantisation force due to resonance, which encourages material to stay within the rings. The figure illustrates the fit of quantisation rule Eq.(5) to these sharp edges and horns. Values of coefficient A (marked at the top) appear to be grouped into multiples of 6, 9 or 16, with rings always bordered by two markers from the same group. For example, rings

(α , β , γ , θ) lie in the 6 group, whereas (δ , ϵ , ζ , η) lie in the 9 group, and (κ , λ) lie in the 16 group. This implies collaboration between each ring's *edges*, resulting in 20 ring edges being described by only 11 values of A. Rings α , θ , and λ have exactly the same width. The A values for *mean* ring positions, (as given in Figure 4), are shown at the bottom by the heavy marker lines.

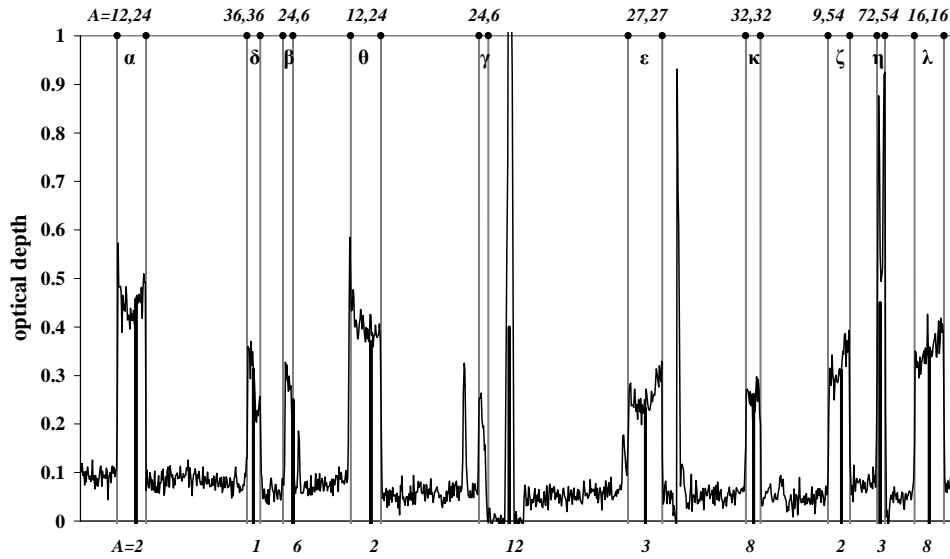


Figure 8. The very strong rings in the outer C Ring ($x = 2401-3520$) have abrupt sides and horns which fit Eq.(5) accurately. Horns indicate that material is encouraged to stay within these rings by resonance inherent in the quantisation phenomenon. It is interesting that the strongest rings (α, θ, λ) have exactly the same width ($\Delta N = 1/8$). The A-values for *mean* ring positions (using Eq.(5) still) are shown at the bottom by the heavy black markers.

The extraordinary strength, regularity, and narrowness of these rings implies that a second law is operating in addition to Eq.(5). A search for this law has revealed a good fit analogous to Eq.(10), based on the proton gravitational de Broglie wavelength:

$$2\pi r = N\alpha^2 \left(\frac{h}{m_p v} \right) \times \left(\frac{e^2}{Gm^2} \right)^{1/2}, \quad (14)$$

Here, the rings are well fitted by N values: $\theta(264)$, $\epsilon(267)$, $\kappa(268)$, $\zeta(269)$, $\lambda(270)$, and second harmonics $\alpha(261.5)$, $\eta(269.5)$. Between θ and ϵ there is a strong narrow

ring at $N = 265.5$, ($A = 12$ from Eq.(5)) located within a cleared ring, probably swept by a moon.

4. Analysis of Saturn's B Ring

The B Ring is full of fine rings superimposed on a high continuum level, but without the regular undulations and strong narrow rings found in the C Ring. First of all, the PPS data was smoothed in order to reveal the low frequency profiles of broader rings. These rings were then fitted satisfactorily to quantisation rule Eq.(5), but were not considered interesting enough to occupy figure space here. Many fine rings were classified as for the C Ring, and it was found that the distribution of A values appears almost random throughout the B Ring. Altogether, 206 significant rings were well fitted with only 21 values of A .

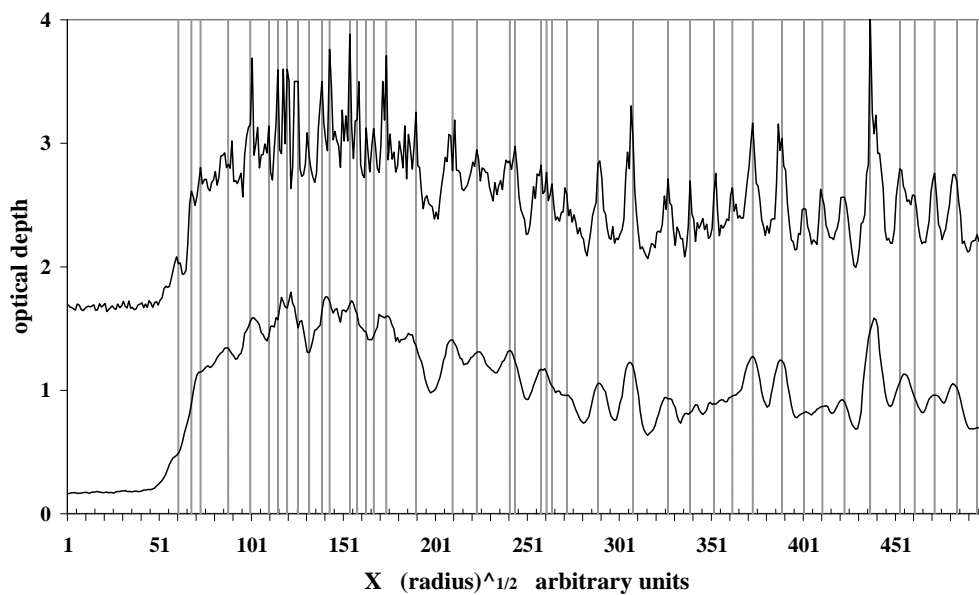


Figure 9. Upper trace: The inner-most B Ring region analyzed at 5km resolution to identify numerous fine rings. Lower trace: Data smoothed over 9 bins are included to reveal how the clustered fine rings shown above may either sit upon broader features or actually constitute them. Some of the broader features become a little sharper in the upper trace but do not resolve significantly further.

As a typical example, the inner-most part of the B Ring was analyzed at 5 km resolution, see Figure 9. Many of the significant rings have been identified, with 14

values of A fitting 47 rings. The underlying continuum level persists, due to material self-gravity filling in between rings, instead of fragmenting into separate fine rings.

The whole B Ring was Fourier transformed in 16 sections of 256 bins each, and revealed some local clumping of A values. However, the *mean* overall spectrum is quite similar to that in the C Ring, see Figure 10. Equation (11) is shown dotted and employs ($y_0 = 1.4$, $A_0 = 1$, and $Q = 0.6$), which indicate that viscous losses are higher in the B Ring, than in the C Ring.

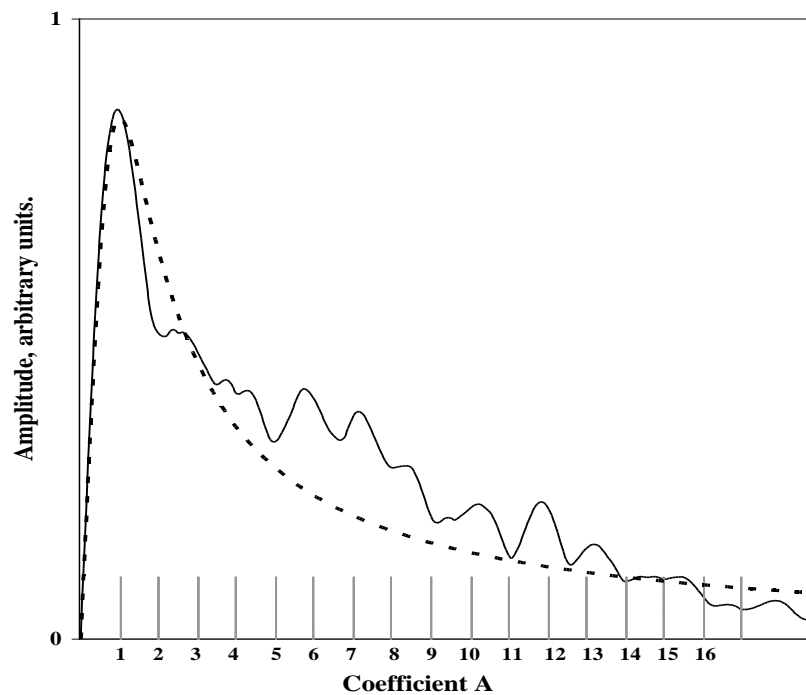


Figure 10. Fourier spectra of 16 adjacent regions in the B Ring, summed to produce a mean spectrum which approximates to a resonance response profile. The real amplitude scale is actually 15 times greater than that for the C Ring of Figure 5, so the quantisation is much stronger.

5. Analysis of Saturn's Cassini division

The Cassini division has several low-level broad rings which may be fitted to Eq.(5), as shown in Figure 11: these are generally located by the ($A=12$) bold marker-lines. Narrow gaps of zero material density exist between the rings, as if possible moons are sweeping-out these orbits, while they also obey Eq.(5). Thirty-three rings in total have been identified with 15 values of A , where coefficient $A=12$ is the most common, implying that resonance coupling exists between the rings.

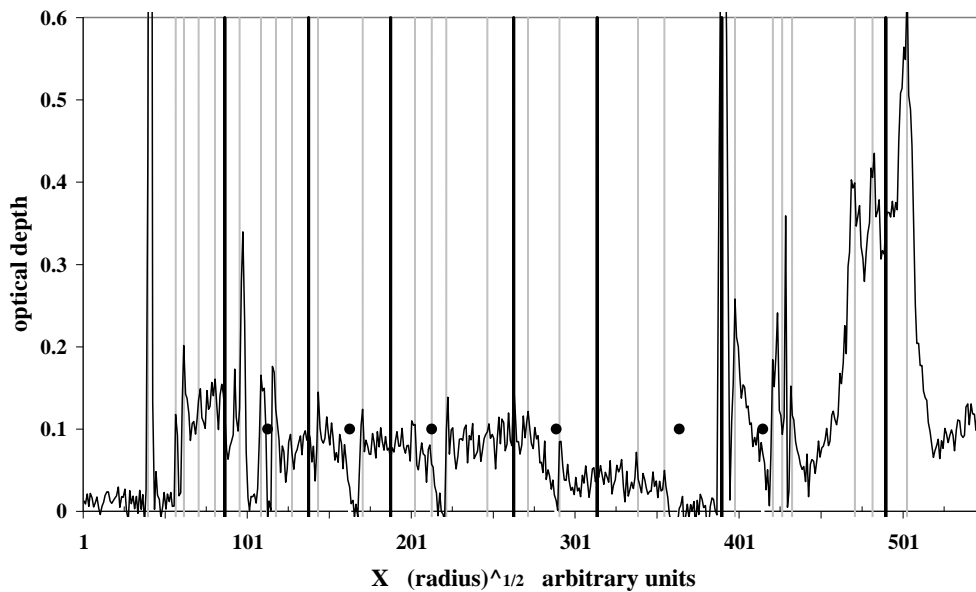


Figure 11. Cassini division analyzed at high resolution (5 km). Periodicity for ($A=12$) is shown by the bold marker lines which align with the lower-level rings. Possible moon positions (the black spots) also fit ($A=12$).

6. Analysis of Saturn's A Ring

The A Ring has few bold features compared with the C and B Rings. After some smoothing, these are shown in Figure 12, with markers for the fit to Eq.(5). Coefficient A as a power of 3 is particularly common, indicating resonance between many rings. A very weak ring within the Encke-gap fits $A = 6$, accurately. The steep walls of the Encke-gap, where main ring material is restored, lie where $A = 4$ and 12. The Keeler-gap also fits $A = 4$. Altogether, 21 rings or edges have been described by only 9 values of A , which appear inter-dependent.

Part of this range, (from $x = 8601$ to 9100 in Figure 2) was analyzed at high resolution to reveal that the many weak fine rings sit upon a large continuum level without cutting into it very much. Coefficient $A = 27$ was strongly preferred.

The A Ring has been Fourier transformed after truncating its strongest features. Eight sections, 256 bins wide were transformed then summed, as illustrated in Figure 13. Equation (11) has again been applied to the mean spectrum (for $y_0 = 1$, $A_0 = 1$, $Q = 0.75$).

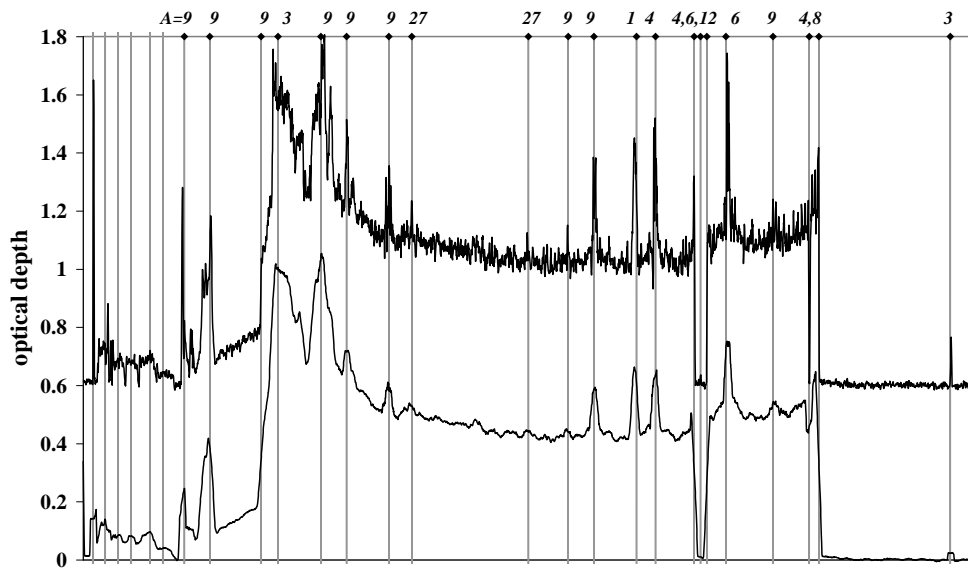


Figure 12. The A Ring analyzed for its main ring features, after 3 bin and 25 bin smoothing. The Cassini division has been included just to illustrate its low frequency periodicity. Note how the sharp rising edges of gaps and boundaries also fit the quantisation rule. Resonance between rings is indicated because coefficient A, as a power of 3 in Eq.(5), is common.

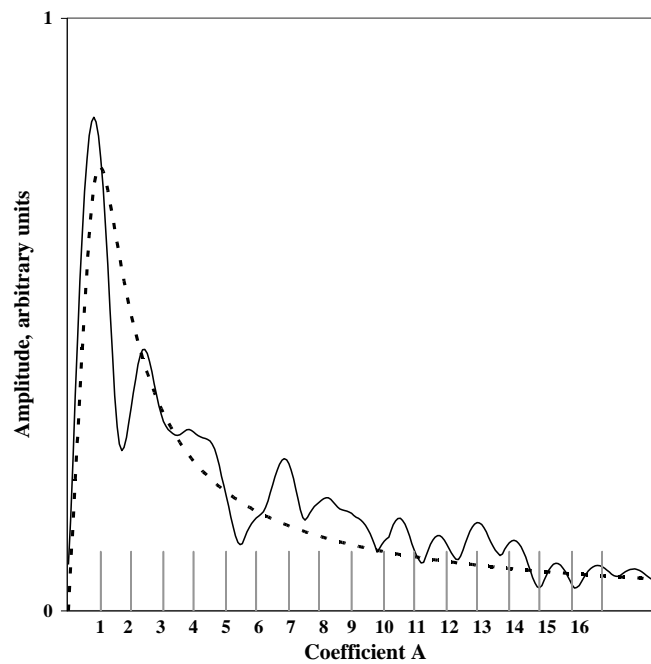


Figure 13. Summed Fourier spectrum for 8 adjacent regions, of 256 bins each, in the A Ring. Strong narrow ring features, plus the Encke gap, were removed to prevent their domination of spectra. A resonance response profile is shown dotted on the mean spectrum.

7. Analysis of Saturn's D Ring

Saturn's D Ring has been studied by Showalter [26], who used two Voyager images to produce radial profiles. These have been scanned then overlaid with ring positions calculated from Eq.(5), as shown in Figure 14. Overall, 29 rings are fitted by only 7 values of A . There is a strong preference for $A = 8$, regularly spaced at around 185 km between D68 and D72, indicating resonance coupling between rings. From D72 to D73 there is some fine ring periodicity of around 125 km spacing ($A = 12$), over a short range. The declining extremities of the D Ring are both featureless, as if the material is too turbulent for rings to form.

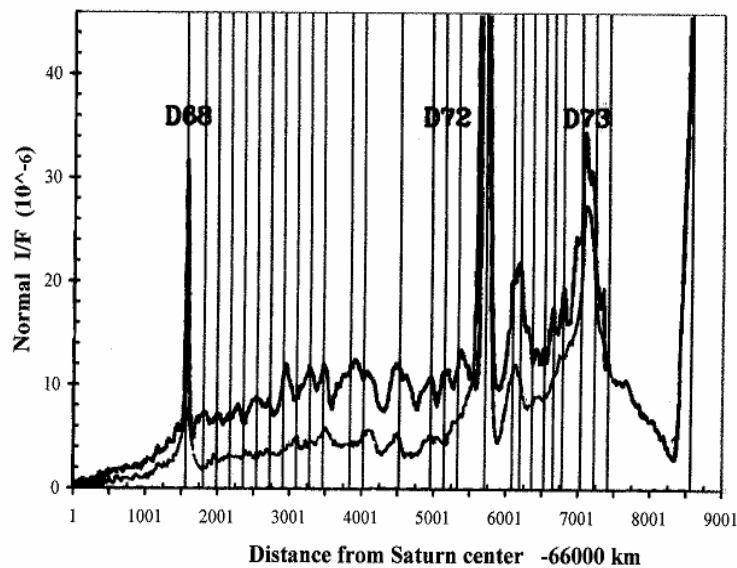


Figure 14. Radial profiles of the D Ring from Voyager 2 (top) and Voyager 1 (bottom), copied from Showalter [26], then overlaid with ring positions calculated from Eq.(5). Periodicity at 185 km is obvious between D68 and D72. Periodicity at 125 km exists over a short range between D68 and D73. Original figure was published in *Icarus*, 124, M. Showalter, Saturn's D Ring in the voyager images, p677, Copyright Elsevier [26].

8. The Rings of Uranus

Ten rings of Uranus, from occultation data provided by NASA, and Loders and Fegley [27], have been fitted individually to Eq.(5), as listed in Table 1. The fit is

accurate, and two values of A (2, 4) cover 10 fine rings, which are eccentric and probably associated with satellite resonances. The apparent regularity of rings 6, 5, 4, requires an explanation, such as:

$$2\pi r = U \left(\frac{h}{m_{\text{H}_2\text{O}} v} \right) \times \left(\frac{e^2}{G m_{\text{H}_2}^2} \right)^{1/2}, \quad (15a)$$

where $m_{\text{H}_2\text{O}}$ is the water molecular mass, so the first bracket is its de Broglie wavelength. Values of U given in Table 1 change by unity for rings 6, 5, 4, in particular, and also change in small steps between other rings. Ring α is the only one requiring second harmonic quantisation. Active involvement of the water molecule (ice) in this manner, for 10 very narrow isolated rings, is remarkable.

Table 1 Analysis of Uranus' rings. a is the measured radius (km).

N/A values for Eq.(5), and U values for Eq.(15a) are given.

| ring | (6) | (5) | (4) | (α) | (β) | (η) | (γ) | (δ) | (λ) | (ϵ) |
|------|-------|-------|-------|--------------|-------------|------------|--------------|--------------|---------------|----------------|
| a = | 41837 | 42235 | 42571 | 44718 | 45661 | 47176 | 47627 | 48299 | 50024 | 51149 |
| N/A= | 372/2 | 747/4 | 375/2 | 769/4 | 777/4 | 395/2 | 793/4 | 799/4 | 813/4 | 411/2 |
| U= | 253 | 254 | 255 | 261.5 | 264 | 269 | 270 | 272 | 277 | 280 |

A very interesting formula describes the *general location* of this whole ring cluster around Uranus:

$$2\pi r = 2 \times 137^4 \left(\frac{h}{m_{\text{H}_2} c} \right) \times \left(\frac{GM_{\text{U}} m_{\text{H}_2}}{\hbar c} \right), \quad (15b)$$

which is centred at $r = 45,461$ km, near ring β . The first bracket is the Compton wavelength for hydrogen molecular mass m_{H_2} . The mass of Uranus is $M_{\text{U}} = 8.682 \times 10^{25}$ kg, and the final term represents a gravitational coupling constant, as in Eq.(2).

9. The Rings of Neptune

Four narrow and one broad rings of Neptune have been fitted individually to Eq.(5), as listed in Table 2. Harmonic coefficient A takes two values (1, 3) to describe the six rings accurately; and values of U for a fit to Eq.(15a) are also given. Surprisingly, the *general location* of this whole ring cluster is also described by Eq.(15b) if $M_{\text{N}} = 1.024 \times 10^{26}$ kg is introduced in place of M_{U} , and then $r = 53, 627$ km.

Table 2 Analysis of Neptune's rings. a is the measured radius (km).

N/A values for Eq.(5), and U values for Eq.(15a) are given.

| ring | Galle | LeVerrier | Arago | anon | Adams |
|------|-------|-----------|-------|-------|-------|
| a = | 41900 | 53200 | 57600 | 62000 | 62933 |
| N/A= | 514/3 | 193/1 | 603/3 | 625/3 | 210/1 |
| U= | 275 | 310 | 322 | 334 | 337 |

The arcs of material in the Adams ring appear rather tenuous and ragged, but may still fit an additional quantisation rule, as follows. Porco [28] has reduced the arc brightness profile to a useful form, and attributed the arcs to a resonant interaction with Galatea. Her Figure 4 has been scanned and superimposed upon our predicted quantisation rule, see Figure 15. In addition to the quantisation force, the accumulation of available arc material will have been governed by turbulence and self-gravity, so the observed missing clumps and filling between the predicted clumps are to be expected.

According to our best fit in Figure 15, there could be 49 arc nodes around the ring, equi-spaced at 7.35deg. There are two interesting empirical formulae for this arrangement of 49 nodes around the ring. First, by analogy with Eq.(2) we have a coupling constant:

$$\frac{GM_N m_{H2}}{\hbar c} \approx \left(\frac{49}{2}\right) \alpha^2 \times \left(\frac{e^2}{Gm_{H2}^2}\right)^{1/2}, \quad (16a)$$

where M_N is Neptune's mass. Second, the circumference of the Adams ring is accurately given by:

$$2\pi r \approx 49 \times \left(\frac{h}{m_q c}\right) \times \left(\frac{e^2}{Gm^2}\right)^{1/2}. \quad (16b)$$

Here, $m_q = m_p/3$ is the quark mass for protons in the arc material; so $(h/m_q c)$ is their equivalent Compton wavelength. The last term is the electromagnetic/gravitational strength ratio, where (e/m) is the electronic charge/mass ratio. Thus, the orbit circumference is equal to 49 quark *gravitational Compton wavelengths*. By analogy, the first Bohr orbit of hydrogen contains 137 electron Compton wavelengths (h/mc) .

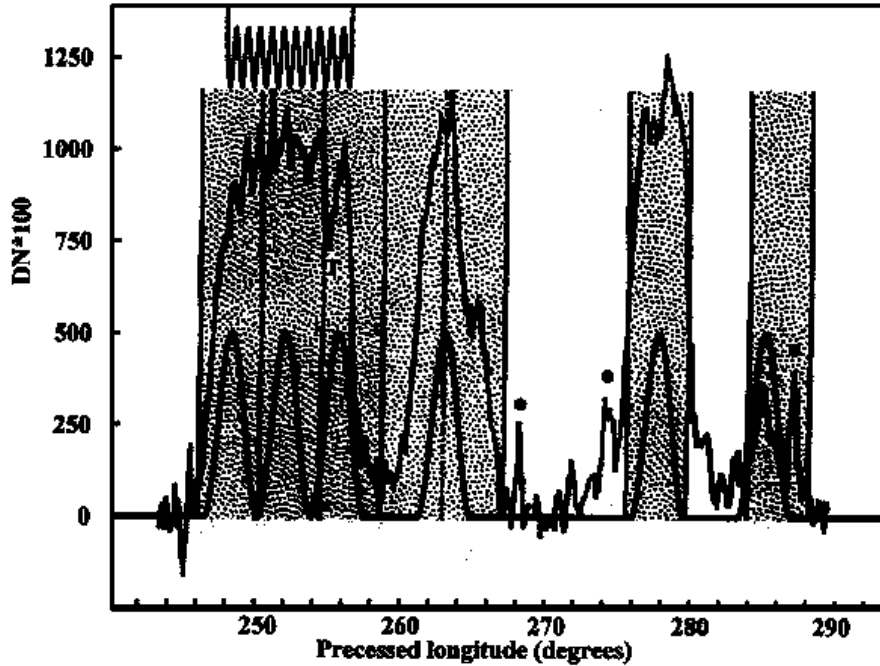


Figure 15. The arc region brightness profile in Neptune's ring, copied from Porco [28] then fitted with Eq.(16). The broad trailing arc may have been filled by harmonic components plus self-gravity. Superimposed fine material clumping indicates 3rd harmonic forces, as simulated at the top-left. Original figure taken from C. Porco, Science 253:995-1000 (30 August 1991) [28]. Reprinted with permission from AAAS.

Small-scale clumping of material, seen in the broad trailing arc, has been fitted very well in Figure 15 top-left to angular interval (7.35deg./ 9). This corresponds with the 3rd harmonic of the proton gravitational Compton wavelength, and would have been selected in cooperation with the local focusing forces mentioned by Porco [28].

10. The Rings of Jupiter

The main component of Jupiter's ring system is spread across radius $r = 126,000$ km, which satisfies an equation somewhat similar to Eq.(15b), namely:

$$2\pi r = N_J \times 137^4 \left(\frac{h}{m_{H_2} c} \right) \times \left(\frac{GM_J m_{H_2}}{\hbar c} \right), \quad (17)$$

where $N_J = 1/4$, and $M_J = 1.899 \times 10^{27}$ kg. Coincidentally, this produces a very good result for our general ring equation (4), when $A=2$:

$$N = \frac{2}{137} \left(\frac{c}{v} \right) = 137 \quad . \quad (18)$$

Table 3 lists the values of N_j at the *observed interfaces* in the ring system, where Jupiter's satellites also orbit.

Table 3 Analysis of Jupiter's rings. a is the measured radius (km), and N_j is the ring/boundary coefficient.

| <u>Ring name</u> | <u>a (km)</u> | <u>N_j</u> |
|--------------------------------|----------------------------|-------------------------|
| Halo inner edge | 100,000 | 1/5 |
| Main ring | 126,000 | 1/4 |
| Gossamer ring transition | 182,000 | 1/3 |
| Outer gossamer ring outer edge | 222,000 | 4/9 |

For comparison purposes, Saturn's extensive ring system is spread across the strong B Ring and satisfies an equation similar to Eq.(17):

$$2\pi r = \left(\frac{3}{4} \right) \times 137^4 \left(\frac{h}{m_{H_2} c} \right) \times \left(\frac{GM_S m_{H_2}}{\hbar c} \right) \quad . \quad (19)$$

Coefficient (3/4) would become (1/2) at the inner boundary of the C Ring. The mass m_{H_2} in this expression could be replaced freely by other atomic or molecular species.

Saturn's tenuous E Ring, which peaks at $r = 235,000\text{km}$ and is maintained by material from Enceladus, also fits Eq.(19) for coefficient (3/2) and arbitrary other species.

The remarkable discovery of an enormous ring around Saturn is also worth including; see Verbiscer, Skrutskie and Hamilton [29]. Observations do not extend over the full ring width but the radius for maximum ring strength is probably around $170 R_S = 10.3 \times 10^6 \text{km}$. For this radius, coefficient (3/4) in Eq.(19) would be replaced by (137/2), which is very satisfactory. Material for the ring is apparently supplied by Phoebe.

11. Conclusion

The prominent ring features in Saturn's ring system, and the rings of other planets, have been fitted to quantisation rules derived from atomic theory. Application of the major rule appears periodic for broad rings, and fits fine rings in batches. The existence of a physical quantisation force is inferred from the obvious

degree of correlation, which has no known classical explanation. Long-term stability is a characteristic of the quantisation phenomenon. Fourier transformation of C, B, and A ring data has produced 3 frequency spectra which fit response profiles characteristic of electro-mechanical resonance systems. Turbulence is probably the main destroyer of the ring quantisation mechanism. Fine rings as narrow as 0.06 km radial width are predicted by this theory, in agreement with the 'record-groove' structure observed. Clumping of material at nodes around orbits is predicted, due to the standing-wave nature of quantisation. The absolute nature of the quantisation rule allows no local adjustments, so the accurate fit to so many rings is very impressive. Successful application of quantisation rules to ring systems of the other planets indicates that the quantisation force is real, rather than it being an artefact of some classical effect within Saturn's system.

Acknowledgements

I would like to thank Imperial College Libraries and R. Glovnea for computing assistance and R. Simpson for typing.

References

1. Cuzzi JN, et al: *Space Science Reviews* 2002, **18**:209-251.
2. Esposito LW: *Rep. Prog. Phys* 2002, **65**:1741-1783.
3. Gordon MK, et al: Planetary Rings in M. V. Sykes (ed), *The Future of Solar System Exploration*, 2003-2013, ASP Conf. Ser 2002, **272**:263-282.
4. Cuzzi JN, Lissauer JJ, Shu FH: *Nature* 1981, **292**:703-707.
5. Lissauer JJ, Shu FH, Cuzzi JN: *Nature* 1981, **292**:707-711.
6. Goldreich P, Tremaine S: *Ann. Rev Astron Astrophys* 1982, **20**:249-283.
7. Holberg JB, Forrester WT, Lissauer JJ: *Nature* 1982, **297**:115-120.
8. Smith BA, et al: *Science* 1982, **215**:504-537.
9. Esposito LW, O'Callaghan M, West RA: *Icarus* 1983, **56**:439-452.
10. Lane AL, Graps AL, Simmons KE: The C Ring of Saturn, in A. Brahic (ed), *Proc. I.A.U. Colloquium 75 Planetary Rings*, Toulouse, France, Aug. 1982, 1983: 251-258.
11. Cuzzi JN, Lissauer JJ, Esposito LW, Holberg JB, Marouf EA, Tyler GL, Boisshot A: Saturn's rings: properties and processes. In *Planetary Rings*, edited by Greenberg R and Brahic A, Tucson, Univ Arisona Press, 1984:73-199.
12. Borderies N, Goldreich P, Tremaine S: *Icarus* 1986, **68**:522-533.
13. Esposito LW: *Icarus* 1986, **67**:345-357.

14. Borderies N: *Publ Astron Inst Czec Sci* 1987, **68**:151-157.
15. Esposito LW, Harris CC, Simmons KE: *Astrophys J Suppl Ser* 1987, **63**:749-770.
16. Nicholson PD, Dones L: *Rev Geophys Sup* 1991, **29**:313.
17. Nicholson PD: Observations of resonance phenomena in planetary rings, 7. *Florida workshop on nonlinear astronomy: astrophysical disks*, 1992:324-339.
18. Horn, LJ, Cuzzi JN: *Icarus* 1996, **119**:285-310.
19. Fridman AM, Gorkavyi NN: *Physics of planetary rings*, Springer Verlag, Berlin 1999.
20. Nicholson PD: *Bull Amer Astro Soc* 2001, **33**:1187.
21. Tiscareno MS, Burns JA, Nicholson PD, Hedman MM, Porco CC: Ring reconnaissance with weak waves, *Amer Geophys Union, Fall Meeting 2006*, abstract No. P34A-02.
22. Wayte R: *Moon and Planets* 1982, **26**:11-32.
23. Nottale L, Schumacher G, Gay J: *Astron Astrophys* 1997, **322**:1018-1025.
24. Rafie F: *Astron Astrophys Transact* 2005, **24**:81-92.
25. Stephenson RJ: *Mechanics and Properties of Matter*, 2nd edition, John Wiley, N.York. 1961:139-147.
26. Showalter MR: *Icarus* 1996, **124**:677.
27. Lodders K, Fegley BJ: *The planetary scientist's companion*, OUP Oxford 1998.
28. Porco CC: *Science* 1991, **253**:995-1001.
29. Verbiscer AJ, Skrutski MF, Hamilton DP: *Nature online* 7 Oct, 2009, Letters 1-3.